ACS NANO

www.acsnano.org

ARTICLE

Nonenzymatic Glucose Sensing Using $Ni_{60}Nb_{40}$ Nanoglass

Soumabha Bag,*,# Ananya Baksi,*,# Sree Harsha Nandam, Di Wang, Xinglong Ye, Jyotirmoy Ghosh, Thalappil Pradeep, and Horst Hahn*

Cite This: *ACS Nano* 2020, 14, 5543–5552

Read Online

ACCESS | Metrics & More | Article Recommendations | Supporting Information

ABSTRACT: **Despite being researched for nearly five decades, chemical application of metallic glass is scarcely explored. Here we show electrochemical nonenzymatic glucose-sensing ability of nickel–niobium ($Ni_{60}Nb_{40}$) amorphous alloys in alkaline medium. Three different $Ni_{60}Nb_{40}$ systems with the same elemental composition, but varying microstructures are created following different synthetic routes and tested for their glucose-sensing performance. Among melt-spun ribbon, nanoglass, and amorphous–crystalline nanocomposite materials, nanoglass showed the best performance in terms of high anodic current density, sensitivity (20 mA cm^{-2} mM^{-1}), limit of detection (100 nM glucose), stability, reproducibility (above 5000 cycles), and sensing accuracy among nonenzymatic glucose sensors involving amorphous alloys. When annealed under vacuum, only the heat-treated nanoglass retained a similar electrochemical-sensing property, while the other materials failed to yield desired results. In nanoglass, a network of glassy interfaces, compared to melt-spun ribbon, is plausibly responsible for the enhanced sensitivity.**

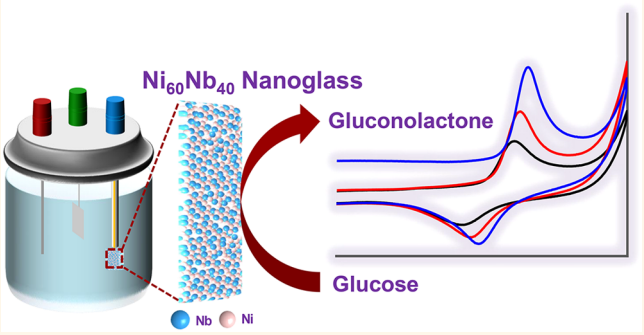

KEYWORDS: *nanoglass, nonenzymatic glucose sensor, nickel–niobium alloy, cyclic voltammetry, electrochemistry*

Accurate glucose detection ability is essential to capture small changes in concentration in order to design advanced clinical diagnostic devices[1,2] (blood sugar analysis apparatus[1−5] and other personal health care devices[6]). Besides clinical applications, environmental,[7,8] food[9−11] and drug quality inspection,[12,13] and bioprocesses[14] monitoring is carried out upon evaluating glucose reactivity. In order to accommodate all the above-mentioned requirements, constant efforts are made to develop a universal sensor, which will be fast, selective, reliable, cost-effective, user-friendly, and efficient. Initially, Clark and Lyons[15] designed an enzyme-based electrode using the specific biocatalytic property of glucose oxidase, or GOx. This was further improved, leading to the development of redox electrodes[16,17] toward clinical diagnosis aimed for point of use in diabetes control. Despite its success, enzymatic glucose sensors possess several problems to address, such as immobilization of GOx on electrodes,[18,19] long-time stability,[20] thermal and chemical stability,[21] handling, and repeated use of the same sensor. Besides clinical diagnostics, a limited range of thermal stability[21,22] (until 44 °C) of GOx-based sensors along with their unstable nature in lower (below 2) and higher (above 8) pH values[18] makes it a poor choice for sensors for commercial use in agriculture and food quality monitoring.[23] In order to address the above-mentioned problems, immense efforts are made to develop effective nonenzymatic glucose-sensing technology based on metals and nanomaterials.

Among different diagnostic patterns invented to monitor glucose concentrations, such as transdermal technology,[24,25] optical[14,26,27] and acoustic,[28] and electrochemistry[29−33] based diagnostic tools have been found to be the most efficient and user-friendly. Generally, electrodes made of noble metals, such as gold,[34] silver,[35] palladium,[36,37] and platinum,[38,39] are used to produce enzyme-free glucose sensors in spite of their high cost. But, all these emerging sensors have been unable to demonstrate sensitivity comparable to GOx-based detectors mainly due to poor electro-oxidation kinetics, despite introducing anisotropic nanostructured electrodes[40−42] or alloying[20,43,44] during the design of the electrode. Therefore, readily available, cost-effective transition metal[3,20] catalysts are

Received: December 12, 2019
Accepted: April 8, 2020
Published: April 8, 2020

https://dx.doi.org/10.1021/acsnano.9b09778
ACS Nano 2020, 14, 5543–5552

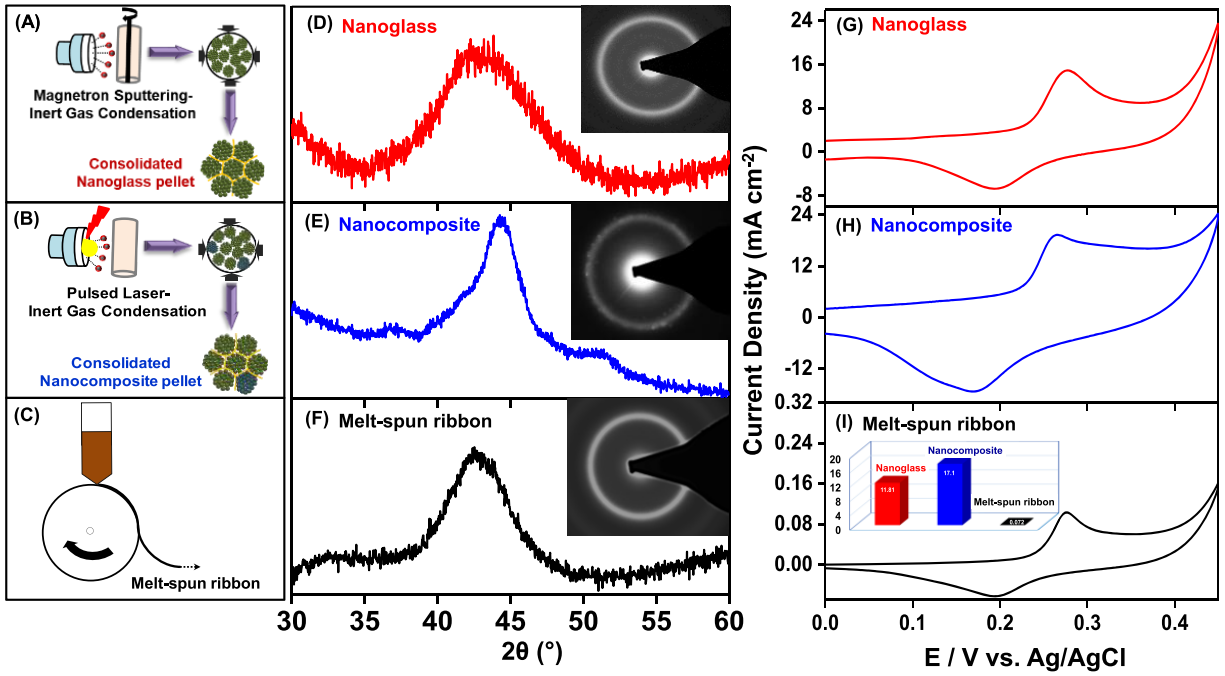

Figure 1. Nonenzymatic glucose sensor based on $Ni_{60}Nb_{40}$ glassy alloy materials is illustrated. Schematics in A to C show preparation methods of nanoglass, nanocomposite, and melt-spun ribbon, respectively. XRD analysis indicates the amorphous phase of the sample (D and F), which are further confirmed through SAED patterns shown in the insets. Cyclic voltammograms of 0.10 mM glucose in 0.1 M sodium hydroxide solution are shown in G–I. Variation of anodic peak current density of all the materials is shown in the inset of I.

selected to design a futuristic enzymeless glucose sensor. Among known metals, nickel-based materials (nickel nanoparticle decorated substrate,[45] anisotropic Ni-structures,[20] multicomponent alloys,[18,46] or hybrid structures[47,48] containing nickel) are chosen because of the stable and reversible Ni(III)/Ni(II) redox system[20,49−51] activity known in alkaline conditions. However, during electrochemical oxidation of glucose, such Ni-based sensors' performance and stability decline over time. The above-mentioned challenges can be addressed by designing a new type of ligand-free Ni-based sensor that is able to survive several electrochemical cycles, easy to handle, and able to detect very low concentrations of glucose reproducibly.

Nanostructured metallic glasses (nanoglasses) gained popularity for their different properties[52−58] compared to bulk metallic glassy[59] analogues. The recent introduction of nanoglass[55] in the family of glassy alloys further improved the mechanical strength,[54] enhanced magnetic properties,[53] *etc.*, compared to bulk metallic glasses. Typically, a nanoglass is prepared by consolidating amorphous alloy nanoparticles at high uniaxial pressures (2−6 GPa),[60] creating a large number of glass−glass interfaces, which are responsible for the distinct properties[61] compared to bulk metallic glass of similar or identical composition. While stable amorphous alloys are being used in several places,[62] only a few attempts are made (organic catalyst,[63] electrocatalysis,[64] and sensor[65]) to utilize the chemical reactivity of such amorphous systems as a replacement for crystalline metals. Nickel-based glassy alloys such as $Ni_{60}Nb_{40}$,[66,67] $Ni_{60}Zr_{40}$,[68,69] $Ni_{60}Ag_{40}$,[70,71] and $Ni_{50}Ti_{50}$[72,73] are well known for their distinct thermal stability and mechanical strength, but they have not been used for unconventional chemical applications.[74] These nickel-based glasses could be an excellent choice to develop futuristic nonenzymatic glucose sensors.

In this paper, we synthesized $Ni_{60}Nb_{40}$ nanoglass and demonstrated its electro-oxidation ability in terms of sensitivity and selectivity in glucose sensing. For comparison, melt-spun ribbon and a nanocomposite of amorphous and crystalline alloy with identical compositions ($Ni_{60}Nb_{40}$) have been investigated for their electrochemical activity. The results from the investigations reveal that all three $Ni_{60}Nb_{40}$ alloys can effectively be used to detect glucose electrochemically in the absence of any enzyme. Among them, the nanoglass showed the highest sensitivity (20 mA cm^{-2} mM^{-1}) reported so far for any nonenzymatic glucose sensor based on Ni-based nanomaterials.

RESULTS AND DISCUSSION

Structural Analysis of the Alloys. Three different $Ni_{60}Nb_{40}$ alloys, namely, nanoglass, a mixture of an amorphous−crystalline nanocomposite alloy, and melt-spun ribbon (MSR), were synthesized following different routes shown in Figure 1A−C (details are in the Experimental Section). Structural characterization of the as-prepared samples was performed using X-ray diffraction (XRD) immediately after each synthesis. Corresponding diffractograms associated with each material are shown in Figure 1D to F. Both nanoglass and MSR show a typical halo peak, indicating an amorphous phase in the samples. Detailed microstructural analysis using FESEM (Figure S1A to C) and TEM was carried out. The amorphous nature of the samples was confirmed during a TEM-selected area electron diffraction (SAED) study, which exhibited broad diffuse rings as shown in the insets of Figure 1D and F. Although there was no clear crystalline peak in the XRD pattern (amorphous−crystalline composite or nanocomposite), the halo was sharper for the nanocomposite materials, suggesting nanocrystallinity (Figure 1E) in the sample. Additionally, distinguished spots identified in the

https://dx.doi.org/10.1021/acsnano.9b09778
ACS Nano 2020, 14, 5543−5552

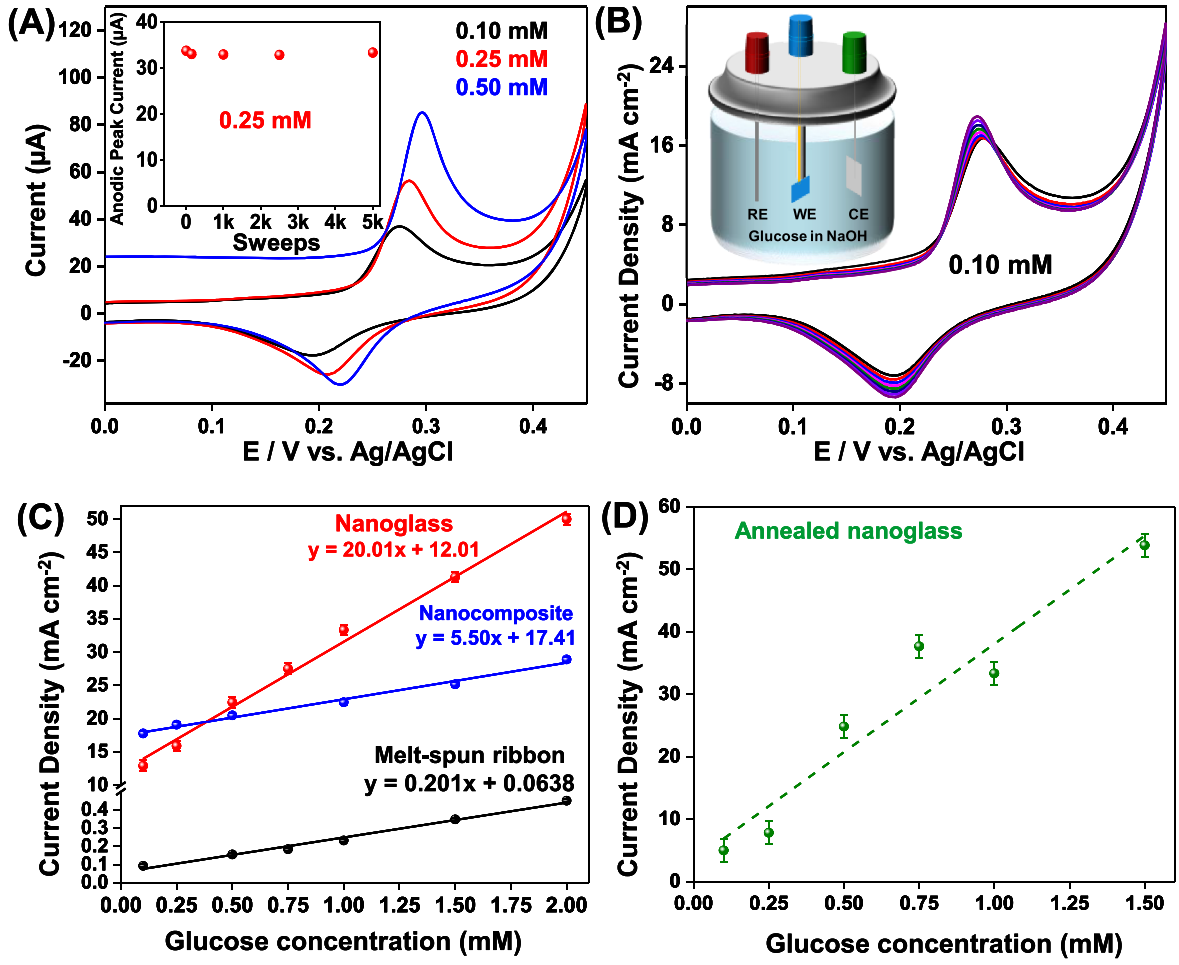

Figure 2. Concentration-dependent (0.10, 0.25, and 0.50 mM glucose) cyclic voltammograms with the nanoglass are shown in A. Stable anodic peak current of a 0.25 mM glucose solution over 5000 cycles is shown in the inset. In B, eight sweeps in a 0.10 mM glucose solution demonstrate stable anodic peak current density. Schematic of the electrochemical cell is shown in the inset of B. In alkaline (NaOH) glucose solution, the reference electrode (Ag/AgCl), working electrode (alloy materials), and counter electrode (platinum foil) are represented by RE, WE, and CE, respectively. Linear dependence on the glucose concentration was found for all three systems, as shown in C, including the equations. Only the annealed nanoglass retained its detection ability and its response, which is captured in D.

SAED (inset of Figure 1E) pattern indicate some extent of nanocrystallinity in the sample.

Electrochemical Stability of the Alloys. After the initial microstructural characterization, these three samples were tested for their electrochemical responses as working electrode (WE) toward glucose in cyclic voltammetry (CV) experiments in the presence of Ag/AgCl as a reference electrode (RE) and platinum as counter electrode (CE) in alkaline medium. The scan rate dependent stability of the alloy electrodes has been checked before initiating any experiment. With the polished glassy electrode, during sweeping from −0.1 to +0.45 V at 10 mV s^{-1} scan rate, oxidative peak in the first cycle indicate the formation of Ni(II) oxide layers.[46] At repeated sweeps using 10 to 100 mV s^{-1} rates the nanoglass electrode produced well-defined and reproducible voltammograms in 0.1 M NaOH solution as shown in Figure S2. Other alloy electrodes also generate a similar voltammetric response. The anodic peak voltage shifts to more positive value with an increase in the scan rate, while reductive peak voltage moves to more negative potential as found in previous studies.[20] During sweeping at a 20 mV s^{-1} rate, the current response was found to be 0.64 μA for the anodic peak at +0.266 V. For a direct comparison between the three materials, the scan rate was fixed at 20 mV s^{-1} for the rest of the experiments. The chemical reactions are as follows[3,20]

$$Ni + 2OH^- \rightarrow Ni(OH)_2 + 2e^-$$

$$Ni(OH)_2 + OH^- \rightarrow NiO(OH) + H_2O + e^-$$

Glucose-Sensing Using Cyclic Voltammetry. In the identical potential regime for nanoglass, upon addition of 0.10 mM glucose solutions into the alkaline medium, a substantial increase in the oxidative peak current was identified in the resultant CV curve, as evident in Figure 1G, and the anodic peak potential shifts to higher voltage. Notable enhancement in anodic peak current is due to the electrochemical oxidation of glucose in the presence of NiO(OH) on the electrode surface. The chemical reaction can be described as

$$\text{glucose} + NiO(OH) \rightarrow \text{gluconolactone} + Ni(OH)_2 + H_2O$$

A comparable sensitivity was measured when the electrode was replaced with the nanocomposite (shown in Figure 1H). Although MSR was able to detect 0.10 mM glucose in solution,

https://dx.doi.org/10.1021/acsnano.9b09778
ACS Nano 2020, 14, 5543−5552

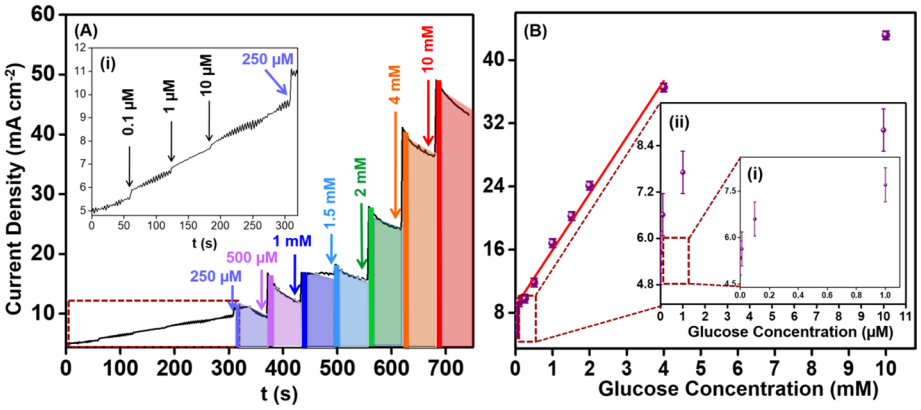

Figure 3. (A) Chronoamperometric response from the nanoglass electrode upon sequential addition of glucose solutions. Inset (i) shows the expanded view of the red dotted region. (B) Distribution of current densities with respect to glucose concentration. A linear increase of current density is established from 0.25 to 4 mM. Current densities at lower concentration are given in insets (i) and (ii).

a weaker oxidative peak current response (inset of Figure 1I) makes it unsuitable for a glucose sensor at the low concentration window (Figure 1I). Appropriate glucose diagnosis is formulated with further CV experiments with different batches of solutions. The gradual increase in the values of the oxidative peak current with increase in glucose concentrations (0.10 to 0.50 mM) clearly indicates the proper sensing response of the nanoglass (Figure 2A). All the CV experiments also produced a very stable anodic peak current. In the inset of Figure 2A, the anodic peak current value of the 0.25 mM glucose solution is shown above 5000 cycles, showing insignificant variation. Additionally, eight replicates of voltammograms from a 0.10 mM glucose solution, shown in Figure 2B, confirm the reproducible nature of every measurement with stable anodic peak current density. Identical measurements were performed on the nanocomposite and MSR, and the sensitivity of these materials was checked with varying glucose concentrations. A linear relationship was found when the anodic peak current density is plotted *vs* glucose concentration (0.10 to 2 mM), and the sensor performance is evaluated for all three alloys (Figure 2C).

The sensitivity values of the alloy sensors are calculated from the slopes shown in Figure 2C, and it is evident that the responses of the nanoglass and the nanocomposite are higher compared to MSR. Although the nanocomposite material shows comparatively higher current density for lower glucose concentration, the current density does not increase tremendously with higher glucose concentration, and hence the overall sensitivity of the nanocomposite materials is lower than the nanoglass (Figure 2C).

Sensitivity of the Nanoglass. Sensitivity of the nanoglass is found to be 20 mA cm^{-2} mM^{-1} (Figure 2C), which is substantially higher compared to other reported nickel-based glucose sensors.[18] The sensitivity of the nanocomposite materials and MSR are 5.5 and 0.2 mA cm^{-2} mM^{-1}, respectively. The current density as well as sensitivity is found to be the lowest for the MSR among all three alloys examined here. It is interesting to note that all three materials showed nearly linear behavior in terms of current response with respect to glucose concentration.

Response from the Annealed Nanoglass. In order to gain more insight into the phase-dependent sensitivity of the materials; all sensors were first annealed at 700 °C [above its glass transition temperature (T_g), 622 °C] for 2 h in a vacuum furnace. Upon crystallization (Figure S3), a mixture of intermetallic compounds of nickel and niobium (Ni_3Nb, Ni_6Nb_7) appears from a single-phase $Ni_{60}Nb_{40}$ nanoglass.[75] When the CVs of all the annealed (crystallized) electrodes are tested, only the annealed nanoglass showed reproducible current density comparable to the parent nanoglass. However, the high sensitivity is lost (Figure 2D) in the crystallized nanoglass, while other materials do not respond at all and fail to produce any anodic peak current. Although the current density is higher for the annealed nanoglass (with respect to the parent nanoglass), the linear behavior is no more perfect [adj. R^2 = 0.905 compared to adj. R^2 = 0.992 for pristine nanoglass, 0.986 for the nanocomposite, and 0.986 for MSR, respectively (adj. = adjusted)]. This study clearly proves the weak sensitivity of the crystalline materials in nonenzymatic glucose-sensing applications in alkaline medium. Due to the higher sensitivity of the pristine and the annealed samples, further studies are focused on the nanoglass only.

Chronoamperometric Detection Ability of Glucose with Nanoglass. To identify the limit of detection of the nanoglass, chronoamperometric experiments were performed from the lowest to highest concentration (0.1 μM to 10 mM) of glucose, and the results are shown in Figure 3. During the measurement, the potential was held constant at +0.45 V while the solution is stirred constantly (200 rpm rate), and the current is monitored upon successive addition of glucose solutions into 0.1 M NaOH medium. The well-defined stepwise current increase upon sequential addition of glucose proves the accurate electro-oxidation response of the nanoglass as a working electrode. Above 10 mM glucose concentration, a negligible increase of current is identified; therefore, the concentration range of the present investigation is chosen until 10 mM (see later). Based on signal-to-noise ratio (S/N) calculation, the nanoglass offers 100 nM glucose as the limit of detection (LOD), as shown in the inset of Figure 3A. A linear increase of the current density with respect to glucose concentration has been established between 0.25 and 4 mM when chronoamperometric current densities are plotted against glucose concentration (Figure 3B). Due to high current density, a few nanomolar glucose concentration is also detectable as shown in Figure 3Bi and ii, which also supports proper detection ability of the nanoglass at a lower concentration range.

Selectivity of the Nanoglass Electrode. In order to demonstrate the ability of the nanoglass as an enzyme-free glucose sensor for future applications, the selectivity is another

https://dx.doi.org/10.1021/acsnano.9b09778
ACS Nano 2020, 14, 5543−5552

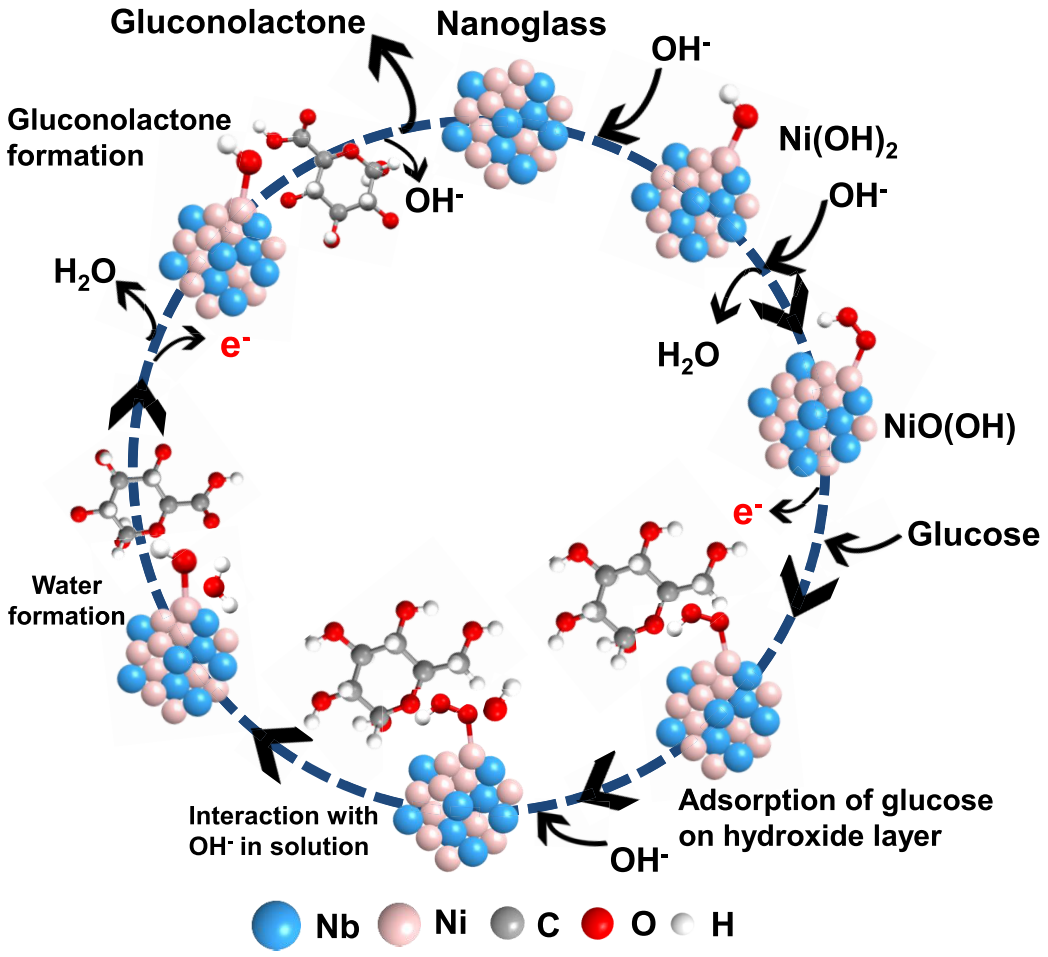

Figure 4. Proposed mechanism of electrochemical glucose oxidation process at the surfaces of the $Ni_{60}Nb_{40}$ nanoglass based on the IHOAM model.

important factor alongside sensitivity, which has to be taken into consideration. Glucose detection is hampered mostly by the presence of sucrose, ascorbic acid, and other solutes in the bloodstream. To perform this test, 0.25 mM ascorbic acid, sodium chloride (NaCl), and a sucrose solutions are added in succession (Figure S4A) in a 0.25 mM glucose solution. A marginal current change upon the addition of other solutes confirms the good selectivity of the nanoglass for glucose. This control test reveals that the nanoglass has potential for accurate glucose detection, and it can be used as a nonenzymatic glucose sensor in future applications. In addition to its selectivity toward glucose detection, the chronoamperometric response of the nanoglass for the sensing of higher glucose concentrations (2 to 38 mM) has also been tested independently (Figure S4B). In identical chronoamperometric experiments (applied potential +0.50 V), the current increases linearly (adj. R^2 = 0.996) with infusion of a higher concentration of glucose until 38 mM. However, above 10 mM, continuous cleaning of the electrodes has been carried out before additional infusion of glucose solution. This problem can be avoided by using a suitable reference electrode, replacing Ag/AgCl.

Post-Experiment Structural Analysis of the Nanoglass. Following the electrochemical studies, structural analysis of the nanoglass electrode was carried out using Ga-XRD to understand the active phase present on its surface. The resultant diffractograms before (Figure S5A) and after (Figure S5B) the reaction showed identical featureless broad peaks, indicating retention of the amorphous phase in the alloy even after electro-oxidation experiments. XRD patterns shown in Figure 1D and Figure S5A were collected from the same sample. The stable nature of the anodic peak current (in the inset of Figure 2A) during the glucose-sensing experiments indicated that chemical composition at the nanoglass surface did not undergo a significant change. Subsequently, surface characterization of the nanoglass was carried out using XPS to determine the chemical composition. The results are summarized in Figure S6. While Figure S6A1, A2, and A3 represent Ni ($2p_{3/2}$), O (1s), and Nb (3d) regions, respectively, of the unreacted nanoglass samples, the same regions of the reacted samples are shown in Figure S6B1, B2, and B3. Nearly the same features are found upon deconvoluting the Ni $2p_{3/2}$ regions (in Figure S6A1 and B1), which also indicates the unaltered surface of the electrode. Careful analysis of the O 1s region points toward different metal−oxygen bonding possibilities at the nanoglass surface (Figure S6A2 and B2), which also do not change significantly following the electro-oxidation process. These features appear mainly due to the presence of amorphous niobium oxide at the surface of the sample, recognized by XPS analysis in the Nb 3d region (Figure S6A3 and B3). Two oxidation states of Nb are found upon deconvoluting two indistinguishable (Figure S6A3 and B3) spectra (dashed lines) measured before and after sensing experiments, respectively. The peak at 203.86 eV is

https://dx.doi.org/10.1021/acsnano.9b09778
ACS Nano 2020, 14, 5543−5552

attributed to the NbO, while the Nb_2O_5 $3d_{5/2}$ signal appears at 207.62 eV. It should be noted that the presence of niobium oxide at the surfaces of the nanoglass has not been identified either by XRD or during TEM/SAED analysis (Figure 1D). The appearance of Ni, Nb, and O peaks from metallic nanoglass suggests the presence of a niobium oxide layer at the surface, which also maintains metallic bonding with Ni[76] but protects underlying Ni−Nb layers from further oxidation. As a result of metallic bonding between Ni and NbO_x at the surface, the oxide layer and the sample remain conducting. This niobium oxide not only facilitates the electrochemical sensing but also shields underlying Ni-excess regions of the sample.

Mechanism. In view of all experimental evidence produced by the electrochemical oxidation process and subsequent spectroscopic characterization of the materials, the nanoglass has emerged as a stable, sensitive, reliable, and robust glucose detector. However, all the studied $Ni_{60}Nb_{40}$ alloy materials have the potential for glucose sensing. The principle reason for such activity is the presence of amorphous nickel with noninterfering and noncompeting niobium in the material. Together these elements produce a stable yet reactive alloy electrode surface for electrochemical glucose sensing. The incipient hydrous oxide adatom mediator (IHOAM)[29,30] model can be used to explain the plausible mechanism (Figure 4) of the oxidation process. According to the reaction mentioned before and this model, a thin layer of nickel hydroxide [$Ni(OH)_2$] forms on the electrode surface in the first sweep of electro-oxidation.[46] $Ni(OH)_2$ subsequently oxidized to nickel oxohydroxide [NiO(OH)] in the alkaline medium, which adsorbs a glucose molecule and gradually converts it to gluconolactone in alkaline conditions. In the process, NiO(OH) reduces to $Ni(OH)_2$ (see Figure 4 for details). Considering the experimental evidence provided here, every working electrode in the current investigations seems to be following the common mechanism formulated using the IHOAM model as shown in Figure 4. In the case of annealed glasses, probably the presence of several intermetallic compounds simultaneously do not help in glucose sensing. Their presence also reduces the metallic bonding between Ni−NbO_x significantly and transforms into a less conducting electrode, which is inefficient for the electrochemical sensing process. The difference in microstructure in the nanoglass and nanocomposite alloy compared to MSR can be another reason for the better electrochemical response among the three materials. In contrast to the melt-spun ribbons, nanoglasses exhibit a network of interfaces. The atomic structure of nanoglasses has been described on the basis of many experiments as to consist of nanometer-sized glassy core regions, *i.e.*, the remnant of the former nanoparticles prior to compaction, and of glassy interfacial regions, which clearly only appear during compaction.[60] The experimental results suggest that the combined reactivity of the two glassy regions, which are characterized by different atomic structures, affects the overall performance of the nanoglass in the sensing application. This is clearly seen in the change of the slope of the current density *vs* the glucose concentration curve (in Figure 2C). The nanoglasses behave distinctively different than the rapidly quenched glass and the nanocomposite materials, both in absolute intensity and in the slope. Both these effects hint toward a different behavior of the interfacial regions present in nanoglasses. Previously, increased mechanical strength (CuZr[54]), altered magnetic properties (FeSc,[53] NiTi[77]), and even enhanced biocompatibility[78] of nanoglasses were correlated with the interfacial regions. The glassy core regions in nanoglasses have similar electrochemical reactivity to that of the melt-spun ribbons. But, the interfacial reactivity in nanoglasses seems to be the main difference, which is reflected as higher current density and sensitivity compared to melt-spun ribbons. On the other hand, the nanocomposite sample consists of glassy, glass−nanocrystalline, and nanocrystalline grains as well as similar interfaces, a combination that might be responsible for the high current density at the lowest glucose concentration. Between nanoglasses and nanocomposite samples, the presence of a larger fraction of glass−glass interfaces is mainly responsible for the higher sensitivity considering the larger concentration range. However, as pointed out above, the change of the slope as seen in Figure 2C indicates additional effects, which cannot be identified based on the present research results.

CONCLUSION

In this report, electrochemical detection of glucose has been demonstrated using nickel-based glassy alloys. Fast, reproducible responses from different $Ni_{60}Nb_{40}$ metallic alloys (nanoglass, nanocomposite, and melt-spun ribbon) are compared for the sensing of glucose solutions. Exceptional response from the nanoglass sample is determined, which retains its partial sensitivity even after annealing and subsequent crystallization. Due to high current density, a few nanomolar glucose is still detectable using a nanoglass electrode. Besides the contribution of metallic nickel, the special nano/microstructure of the nanoglass with interfacial regions of enhanced free volume (interfaces) also seems to play a role in the electrochemical response. A conducting niobium oxide layer coating creates a protection for the Ni-rich alloy but maintains chemical reactivity toward glucose. Based on the IHOAM model, a glucose oxidation mechanism is provided, but further structural insights are necessary to establish it. With a detection limit of 100 nM, the nanoglass has been shown to be an unconventional, nanostructured and ligand-free material to design a futuristic nonenzymatic glucose sensor. An impressive performance of this type of unconventional yet responsive alloy-based sensor has great potential toward the development of diagnostic apparatus and technology to monitor glucose concentrations in challenging application fields.

EXPERIMENTAL SECTION

Chemicals. $Ni_{60}Nb_{40}$ target (99.9% purity) was purchased from MaTeck GmbH. Glucose (99% purity) was procured from VWR GmbH. Sodium hydroxide (NaOH), ascorbic acid, sodium chloride (NaCl), and sucrose with 99.9% purity were purchased from Sigma-Aldrich. Deoxygenated Milli-Q water (18.3 MΩ) was used throughout the experiments.

Synthesis. Synthetic schemes are illustrated in Figure 1 (A to C). Briefly, melt-spun ribbons were prepared by rapid quenching of a molten alloy of Ni and Nb with a 60:40 atomic ratio on a rotating Cu disk. The other samples were synthesized using inert gas condensation (IGC) techniques using two custom-built instruments followed by uniaxial compaction. $Ni_{60}Nb_{40}$ nanoglass was prepared by using magnetron sputtering-IGC (MS-IGC) followed by compaction at 1.4 GPa under vacuum.[54] Here, the $Ni_{60}Nb_{40}$ alloy target was sputtered at an aggregation pressure of 0.3 mbar, which leads to the formation of very fine nanoparticles of the same composition. The nanoparticles were then collected and pressed *in situ* at a pressure of 1.4 GPa to make a disc-shaped pellet. The sample was further consolidated at 6 GPa and polished mechanically (pellet diameter 8 mm, thickness 0.21

https://dx.doi.org/10.1021/acsnano.9b09778
ACS Nano 2020, 14, 5543−5552

mm, weight ~100 mg from 90 min of sputtering) at ambient conditions before studying its electro-oxidation property. The amorphous−crystalline nanocomposite sample was prepared using pulsed laser (20 W laser power) ablation (on the same $Ni_{60}Nb_{40}$ alloy target) setup coupled to an IGC instrument followed by successive consolidation at 1.8 and 6 GPa.[79] A disc-shaped pellet was prepared and polished similar to the previous nanoglass sample. The use of pulsed laser ablation instead of magnetron sputtering in the IGC system induced nanocrystallinity in the compacted pellet.

Electrochemical Cell Configuration. All the electrochemical (cyclic voltammetry and chronoamperometry) experiments were performed in a general-purpose electrochemical system (from μAutolab Type III) coupled with a three-electrode electrochemical cell, where $Ni_{60}Nb_{40}$ alloys were used as working electrode, platinum foil as counter electrode, and saturated Ag/AgCl as reference electrode. A gold wire of 0.10 mm thickness was used to connect working electrodes (pellets of nanoglass, nanocomposite, or melt-spun ribbon).

Cyclic Voltammetry and Chronoamperometry. Cyclic voltammetric and chronoamperometric studies were performed with different concentrations of glucose solutions (100 nM to 38 mM, generated more than a few thousand sensing experiments with a single nanoglass electrode) prepared in 0.1 M NaOH at room temperature (25 °C) in a 50 mL cell (schematically shown in the inset of Figure 2B). Scan voltage was fixed between −0.1 and +0.45 V to avoid any interference emerging from niobium. During chronoamperometric measurement, glucose, ascorbic acid, sodium chloride (NaCl), and sucrose solutions were added into a 0.1 M NaOH solution sequentially with constant stirring at 200 rpm. The geometric surface area of the working electrodes (alloys) was used to calculate the current density values reported here. All the potential values described in this paper were determined with respect to the saturated Ag/AgCl electrode.

Characterization. Conventional characterization techniques were used to determine the phase and composition of the as-prepared materials. Structural characterization (XRD) of the metallic alloys was carried out using a Bruker X-ray diffractometer equipped with a Cu Kα X-ray source before attempting electrochemical studies. A STOE Stadi P diffractometer with a Ga Kβ source was used for Ga-jet XRD characterization of the reacted electrode. Microstructure analysis was performed using a Zeiss LEO 1530 scanning electron microscope and an image aberration-corrected FEI Titan 80-300 transmission electron microscope operated at 300 kV. Elemental analysis and chemical compositions ($Ni_{60}Nb_{40}$) were determined with an energy dispersive X-ray spectroscopy detector attached to the SEM and TEM instruments. X-ray photoelectron spectroscopy (XPS) measurement was carried out in an ECSA probe TPD spectrometer from Omicron Nanotechnology with polychromatic Al Kα ($h\nu$ = 1486.6 eV) as X-ray source. All XPS spectra were deconvoluted and analyzed using CasaXPS software.

ASSOCIATED CONTENT

Supporting Information

The Supporting Information is available free of charge at https://pubs.acs.org/doi/10.1021/acsnano.9b09778.

FESEM, CV, selectivity test of the nanoglass, and additional characterization before and after the electro-oxidation reaction such as XRD and XPS (PDF)

AUTHOR INFORMATION

Corresponding Authors

Soumabha Bag − *Institute of Nanotechnology, Karlsruhe Institute of Technology, 76344 Eggenstein-Leopoldshafen, Germany;* orcid.org/0000-0002-0932-105X; Email: soumabha.bag@kit.edu

Ananya Baksi − *Institute of Nanotechnology, Karlsruhe Institute of Technology, 76344 Eggenstein-Leopoldshafen, Germany;* orcid.org/0000-0003-3328-4399; Email: ananya.baksi@kit.edu

Horst Hahn − *Institute of Nanotechnology, Karlsruhe Institute of Technology, 76344 Eggenstein-Leopoldshafen, Germany; KIT-TUD Joint Research Laboratory Nanomaterials, 64206 Darmstadt, Germany;* orcid.org/0000-0001-9901-3861; Email: horst.hahn@kit.edu

Authors

Sree Harsha Nandam − *Institute of Nanotechnology, Karlsruhe Institute of Technology, 76344 Eggenstein-Leopoldshafen, Germany*

Di Wang − *Institute of Nanotechnology and Karlsruhe Nano Micro Facility, Karlsruhe Institute of Technology, 76344 Eggenstein-Leopoldshafen, Germany;* orcid.org/0000-0001-9817-7047

Xinglong Ye − *Institute of Nanotechnology, Karlsruhe Institute of Technology, 76344 Eggenstein-Leopoldshafen, Germany*

Jyotirmoy Ghosh − *Department of Science and Technology (DST) Unit of Nanoscience and Thematic Unit of Excellence (TUE), Department of Chemistry, Indian Institute of Technology Madras, Chennai 600036, India*

Thalappil Pradeep − *Department of Science and Technology (DST) Unit of Nanoscience and Thematic Unit of Excellence (TUE), Department of Chemistry, Indian Institute of Technology Madras, Chennai 600036, India;* orcid.org/0000-0003-3174-534X

Complete contact information is available at: https://pubs.acs.org/10.1021/acsnano.9b09778

Author Contributions

#S. Bag and A. Baksi contributed equally.

Author Contributions

A.B. and S.B. jointly planned and performed the experiments and interpreted the results. S.H.N. helped in magnetron sputtering experiments. D.W. performed the TEM characterization and helped in microstructure analysis. X.L.Y. helped to design initial electrochemical experiments. The XPS was done in collaboration with T.P. and his group. J.G. carried out XPS measurement and analysis. H.H. supervised the entire project. A.B., S.B., and H.H. wrote the manuscript with contributions from other authors.

Notes

The authors declare no competing financial interest.

ACKNOWLEDGMENTS

S.B. and A.B. gratefully acknowledge Karlsruhe Institute of Technology for guest scientist fellowships. H.H. and S.H.N. acknowledge the financial support provided by the Deutsche Forschungsgemeinschaft under grant HA 1344/30-2. S.B. and A.B. thank Dr. Robert Kruk for scientific support. J.G. thanks the University Grants Commission (UGC), India, for his research fellowship. T.P. thanks Department of Science and Technology (DST), India, for the research support. The authors would like to thank Dr. Zbigniew Śniadecki from Institute of Molecular Physics, Polish Academy of Sciences, Poland, for the melt-spun ribbon sample. Dr. Ben Breitung is gratefully acknowledged for the Ga-jet XRD measurements.

REFERENCES

(1) Heller, A.; Feldman, B. Electrochemical Glucose Sensors and Their Applications in Diabetes Management. *Chem. Rev.* **2008**, *108*, 2482−2505.

(2) Harper, A.; Anderson, M. R. Electrochemical Glucose Sensors - Developments Using Electrostatic Assembly and Carbon Nanotubes for Biosensor Construction. *Sensors* **2010**, *10*, 8248−8274.

(3) Tian, K.; Prestgard, M.; Tiwari, A. A Review of Recent Advances in Nonenzymatic Glucose Sensors. *Mater. Sci. Eng., C* **2014**, *41*, 100−118.

(4) Ahmad, R.; Tripathy, N.; Park, J.-H.; Hahn, Y.-B. A Comprehensive Biosensor Integrated with a ZnO Nanorod FET Array for Selective Detection of Glucose, Cholesterol and Urea. *Chem. Commun.* **2015**, *51*, 11968−11971.

(5) Ahmad, R.; Ahn, M.-S.; Hahn, Y.-B. Fabrication of a Non-Enzymatic Glucose Sensor Field-Effect Transistor Based on Vertically-Oriented ZnO Nanorods Modified with Fe_2O_3. *Electrochem. Commun.* **2017**, *77*, 107−111.

(6) Alfian, G.; Syafrudin, M.; Ijaz, M. F.; Syaekhoni, M. A.; Fitriyani, N. L.; Rhee, J. A Personalized Healthcare Monitoring System for Diabetic Patients by Utilizing BLE-Based Sensors and Real-Time Data Processing. *Sensors* **2018**, *18*, 2183.

(7) Bandiello, E.; Sessolo, M.; Bolink, H. J. Aqueous Electrolyte-Gated ZnO Transistors for Environmental and Biological Sensing. *J. Mater. Chem. C* **2014**, *2*, 10277−10281.

(8) Sardesai, N. P.; Karimi, A.; Andreescu, S. Engineered Pt-Doped Nanoceria for Oxidase-Based Bioelectrodes Operating in Oxygen-Deficient Environments. *ChemElectroChem* **2014**, *1*, 2082−2088.

(9) Amor-Gutierrez, O.; Costa Rama, E.; Costa-Garcia, A.; Fernandez-Abedul, M. T. Paper-Based Maskless Enzymatic Sensor for Glucose Determination Combining Ink and Wire Electrodes. *Biosens. Bioelectron.* **2017**, *93*, 40−45.

(10) Liu, Y.; Javvaji, V.; Raghavan, S. R.; Bentley, W. E.; Payne, G. F. Glucose Oxidase-Mediated Gelation: A Simple Test to Detect Glucose in Food Products. *J. Agric. Food Chem.* **2012**, *60*, 8963−8967.

(11) Baksi, A.; Gandi, M.; Chaudhari, S.; Bag, S.; Sen Gupta, S.; Pradeep, T. Extraction of Silver by Glucose. *Angew. Chem., Int. Ed.* **2016**, *55*, 7777−7781.

(12) Balaconis, M. K.; Billingsley, K.; Dubach, M. J.; Cash, K. J.; Clark, H. A. The Design and Development of Fluorescent Nano-Optodes for *In Vivo* Glucose Monitoring. *J. Diabetes Sci. Technol.* **2011**, *5*, 68−75.

(13) Elshaarani, T.; Yu, H.; Wang, L.; Zain ul, A.; Ullah, R. S.; Haroon, M.; Ullah Khan, R.; Fahad, S.; Khan, A.; Nazir, A.; Usman, M.; Naveed, K.-u.-R. Synthesis of Hydrogel-Bearing Phenylboronic Acid Moieties and Their Applications in Glucose Sensing and Insulin Delivery. *J. Mater. Chem. B* **2018**, *6*, 3831−3854.

(14) Steiner, M.-S.; Duerkop, A.; Wolfbeis, O. S. Optical Methods for Sensing Glucose. *Chem. Soc. Rev.* **2011**, *40*, 4805−4839.

(15) Clark, L. C., Jr.; Lyons, C. Electrode Systems for Continuous Monitoring in Cardiovascular Surgery. *Ann. N. Y. Acad. Sci.* **1962**, *102*, 29−45.

(16) Updike, S. J.; Hicks, G. P. Enzyme Electrode. *Nature* **1967**, *214*, 986−988.

(17) Updike, S. J.; Hicks, G. P. Reagentless Substrate Analysis with Immobilized Enzymes. *Science* **1967**, *158*, 270−272.

(18) Toghill, K. E.; Compton, R. G. Electrochemical Non-Enzymatic Glucose Sensors: A Perspective and An Evaluation. *Int. J. Electrochem. Sci.* **2010**, *5*, 1246−1301.

(19) Park, S.; Boo, H.; Chung, T. D. Electrochemical Non-Enzymatic Glucose Sensors. *Anal. Chim. Acta* **2006**, *556*, 46−57.

(20) Niu, X.; Lan, M.; Zhao, H.; Chen, C. Highly Sensitive and Selective Nonenzymatic Detection of Glucose Using Three-Dimensional Porous Nickel Nanostructures. *Anal. Chem.* **2013**, *85*, 3561−3569.

(21) Li, J.; Lin, X. Glucose Biosensor Based on Immobilization of Glucose Oxidase in Poly(*o*-Aminophenol) Film on Polypyrrole-Pt Nanocomposite Modified Glassy Carbon Electrode. *Biosens. Bioelectron.* **2007**, *22*, 2898−2905.

(22) Wilson, R.; Turner, A. P. F. Glucose Oxidase: An Ideal Enzyme. *Biosens. Bioelectron.* **1992**, *7*, 165−185.

(23) Niu, X. H.; Shi, L. B.; Zhao, H. L.; Lan, M. B. Advanced Strategies for Improving the Analytical Performance of Pt-Based Nonenzymatic Electrochemical Glucose Sensors: A Minireview. *Anal. Methods* **2016**, *8*, 1755−1764.

(24) Kost, J.; Mitragotri, S.; Gabbay, R. A.; Pishko, M.; Langer, R. Transdermal Monitoring of Glucose and Other Analytes Using Ultrasound. *Nat. Med.* **2000**, *6*, 347−350.

(25) Lee, H.; Song, C.; Hong, Y. S.; Kim, M. S.; Cho, H. R.; Kang, T.; Shin, K.; Choi, S. H.; Hyeon, T.; Kim, D.-H. Wearable/Disposable Sweat-Based Glucose Monitoring Device with Multistage Transdermal Drug Delivery Module. *Sci. Adv.* **2017**, *3*, e1601314/1−e1601314/8.

(26) Larin, K. V.; Eledrisi, M. S.; Motamedi, M.; Esenaliev, R. O. Noninvasive Blood Glucose Monitoring with Optical Coherence Tomography. A Pilot Study in Human Subjects. *Diabetes Care* **2002**, *25*, 2263−2267.

(27) Zhang, C.; Cano, G. G.; Braun, P. V. Linear and Fast Hydrogel Glucose Sensor Materials Enabled by Volume Resetting Agents. *Adv. Mater.* **2014**, *26*, 5678−5683.

(28) Weiss, R.; Yegorchikov, Y.; Shusterman, A.; Raz, I. Noninvasive Continuous Glucose Monitoring Using Photoacoustic Technology - Results from the First 62 Subjects. *Diabetes Technol. Ther.* **2007**, *9*, 68−74.

(29) Burke, L. D. Premonolayer Oxidation and Its Role in Electrocatalysis. *Electrochim. Acta* **1994**, *39*, 1841−1848.

(30) Rahman, M. M.; Ahammad, A. J. S.; Jin, J.-H.; Ahn, S. J.; Lee, J.-J. A Comprehensive Review of Glucose Biosensors Based on Nanostructured Metal-Oxides. *Sensors* **2010**, *10*, 4855−4886.

(31) Ahmad, R.; Ahn, M.-S.; Bhat, K. S.; Mahmoudi, T.; Wang, Y.; Yoo, J.-Y.; Kwon, D.-W.; Yang, H.-Y.; Hahn, Y.-B.; Tripathy, N. Highly Efficient Non-Enzymatic Glucose Sensor Based on CuO Modified Vertically-Grown ZnO Nanorods on Electrode. *Sci. Rep.* **2017**, *7* (1−10), 5715.

(32) Ahmad, R.; Vaseem, M.; Tripathy, N.; Hahn, Y.-B. Wide Linear-Range Detecting Nonenzymatic Glucose Biosensor Based on CuO Nanoparticles Inkjet-Printed on Electrodes. *Anal. Chem.* **2013**, *85*, 10448−10454.

(33) Bhat, K. S.; Ahmad, R.; Yoo, J.-Y.; Hahn, Y.-B. Nozzle-Jet Printed Flexible Field-Effect Transistor Biosensor for High Performance Glucose Detection. *J. Colloid Interface Sci.* **2017**, *506*, 188−196.

(34) Xie, F.; Huang, Z.; Chen, C.; Xie, Q.; Huang, Y.; Qin, C.; Liu, Y.; Su, Z.; Yao, S. Preparation of Au-Film Electrodes in Glucose-Containing Au-Electroplating Aqueous Bath for High-Performance Nonenzymatic Glucose Sensor and Glucose/O_2 Fuel Cell. *Electrochem. Commun.* **2012**, *18*, 108−111.

(35) Baciu, A.; Pop, A.; Remes, A.; Manea, F.; Burtica, G. Non-Enzymatic Electrochemical Determination of Glucose on Silver-Doped Zeolite-CNT Composite Electrode. *Adv. Sci., Eng. Med.* **2011**, *3*, 13−19.

(36) Lu, J.; Do, I.; Drzal, L. T.; Worden, R. M.; Lee, I. Nanometal-Decorated Exfoliated Graphite Nanoplatelet Based Glucose Biosensors with High Sensitivity and Fast Response. *ACS Nano* **2008**, *2*, 1825−1832.

(37) Zhong, X.; Yuan, R.; Chai, Y. *In Situ* Spontaneous Reduction Synthesis of Spherical Pd@Cys-C_{60} Nanoparticles and Its Application in Nonenzymatic Glucose Biosensors. *Chem. Commun.* **2012**, *48*, 597−599.

(38) Yuan, J.; Wang, K.; Xia, X. Highly Ordered Platinum-Nanotubule Arrays for Amperometric Glucose Sensing. *Adv. Funct. Mater.* **2005**, *15*, 803−809.

(39) Park, S.; Chung, T. D.; Kim, H. C. Nonenzymatic Glucose Detection Using Mesoporous Platinum. *Anal. Chem.* **2003**, *75*, 3046−3049.

(40) Song, Y.-Y.; Zhang, D.; Gao, W.; Xia, X.-H. Nonenzymatic Glucose Detection by Using a Three-Dimensionally Ordered, Macroporous Platinum Template. *Chem. - Eur. J.* **2005**, *11*, 2177−2182.

https://dx.doi.org/10.1021/acsnano.9b09778
ACS Nano 2020, 14, 5543−5552

(41) Dawson, K.; Baudequin, M.; O'Riordan, A. Single On-Chip Gold Nanowires for Electrochemical Biosensing of Glucose. *Analyst* **2011**, *136*, 4507−4513.
(42) Jung, D.-U.-J.; Ahmad, R.; Hahn, Y.-B. Nonenzymatic Flexible Field-Effect Transistor Based Glucose Sensor Fabricated Using NiO Quantum Dots Modified ZnO Nanorods. *J. Colloid Interface Sci.* **2018**, *512*, 21−28.
(43) Zhu, C.; Guo, S.; Dong, S. PdM (M = Pt, Au) Bimetallic Alloy Nanowires with Enhanced Electrocatalytic Activity for Electro-Oxidation of Small Molecules. *Adv. Mater.* **2012**, *24*, 2326−2331.
(44) Gao, H.; Xiao, F.; Ching, C. B.; Duan, H. One-Step Electrochemical Synthesis of PtNi Nanoparticle-Graphene Nanocomposites for Nonenzymatic Amperometric Glucose Detection. *ACS Appl. Mater. Interfaces* **2011**, *3*, 3049−3057.
(45) You, T.; Niwa, O.; Chen, Z.; Hayashi, K.; Tomita, M.; Hirono, S. An Amperometric Detector Formed of Highly Dispersed Ni Nanoparticles Embedded in a Graphite-Like Carbon Film Electrode for Sugar Determination. *Anal. Chem.* **2003**, *75*, 5191−5196.
(46) Luo, P. F.; Kuwana, T. Nickel-Titanium Alloy Electrode as a Sensitive and Stable LCEC Detector for Carbohydrates. *Anal. Chem.* **1994**, *66*, 2775−2782.
(47) Wang, C.; Yin, L.; Zhang, L.; Gao, R. Ti/TiO_2 Nanotube Array/Ni Composite Electrodes for Nonenzymatic Amperometric Glucose Sensing. *J. Phys. Chem. C* **2010**, *114*, 4408−4413.
(48) Hui, S.; Zhang, J.; Chen, X.; Xu, H.; Ma, D.; Liu, Y.; Tao, B. Study of an Amperometric Glucose Sensor Based on Pd-Ni/SiNW Electrode. *Sens. Actuators, B* **2011**, *155*, 592−597.
(49) Karikalan, N.; Velmurugan, M.; Chen, S.-M.; Karuppiah, C. Modern Approach to the Synthesis of $Ni(OH)_2$ Decorated Sulfur Doped Carbon Nanoparticles for the Nonenzymatic Glucose Sensor. *ACS Appl. Mater. Interfaces* **2016**, *8*, 22545−22553.
(50) Chen, T.; Liu, D.; Lu, W.; Wang, K.; Du, G.; Asiri, A. M.; Sun, X. Three-Dimensional Ni_2P Nanoarray: An Efficient Catalyst Electrode for Sensitive and Selective Nonenzymatic Glucose Sensing with High Specificity. *Anal. Chem.* **2016**, *88*, 7885−7889.
(51) Urgunde, A. B.; Kumar, A. R.; Shejale, K. P.; Sharma, R. K.; Gupta, R. Metal Wire Networks Functionalized with Nickel Alkanethiolate for Transparent and Enzymeless Glucose Sensors. *ACS Appl. Nano Mater.* **2018**, *1*, 5571−5580.
(52) Fang, J. X.; Vainio, U.; Puff, W.; Wuerschum, R.; Wang, X. L.; Wang, D.; Ghafari, M.; Jiang, F.; Sun, J.; Hahn, H.; Gleiter, H. Atomic Structure and Structural Stability of $Sc_{75}Fe_{25}$ Nanoglasses. *Nano Lett.* **2012**, *12*, 458−463.
(53) Witte, R.; Feng, T.; Fang, J. X.; Fischer, A.; Ghafari, M.; Kruk, R.; Brand, R. A.; Wang, D.; Hahn, H.; Gleiter, H. Evidence for Enhanced Ferromagnetism in an Iron-Based Nanoglass. *Appl. Phys. Lett.* **2013**, *103*, 073106/1−073106/5.
(54) Nandam, S. H.; Ivanisenko, Y.; Schwaiger, R.; Sniadecki, Z.; Mu, X.; Wang, D.; Chellali, R.; Boll, T.; Kilmametov, A.; Bergfeldt, T.; Gleiter, H.; Hahn, H. Cu-Zr Nanoglasses: Atomic Structure, Thermal Stability and Indentation Properties. *Acta Mater.* **2017**, *136*, 181−189.
(55) Gleiter, H. Nanoglasses: A New Kind of Noncrystalline Materials. *Beilstein J. Nanotechnol.* **2013**, *4*, 517−533.
(56) Chen, N.; Louzguine-Luzgin, D. V.; Yao, K. A New Class of Non-Crystalline Materials: Nanogranular Metallic Glasses. *J. Alloys Compd.* **2017**, *707*, 371−378.
(57) Ghafari, M.; Hahn, H.; Gleiter, H.; Sakurai, Y.; Itou, M.; Kamali, S. Evidence of Itinerant Magnetism in a Metallic Nanoglass. *Appl. Phys. Lett.* **2012**, *101*, 243104/1−243104/4.
(58) Singh, S. P.; Chellali, M. R.; Velasco, L.; Ivanisenko, Y.; Boltynjuk, E.; Gleiter, H.; Hahn, H. Deformation-Induced Atomic Rearrangements and Crystallization in the Shear Bands of a $Tb_{75}Fe_{25}$ Nanoglass. *J. Alloys Compd.* **2020**, *821*, 153486.
(59) Wang, W. H.; Dong, C.; Shek, C. H. Bulk Metallic Glasses. *Mater. Sci. Eng., R* **2004**, *R44*, 45−89.
(60) Danilov, D.; Hahn, H.; Gleiter, H.; Wenzel, W. Mechanisms of Nanoglass Ultrastability. *ACS Nano* **2016**, *10*, 3241−3247.
(61) Wang, J. Q.; Chen, N.; Liu, P.; Wang, Z.; Louzguine-Luzgin, D. V.; Chen, M. W.; Perepezko, J. H. The Ultrastable Kinetic Behavior of an Au-Based Nanoglass. *Acta Mater.* **2014**, *79*, 30−36.
(62) Li, J.; Doubek, G.; McMillon-Brown, L.; Taylor, A. D. Recent Advances in Metallic Glass Nanostructures: Synthesis Strategies and Electrocatalytic Applications. *Adv. Mater.* **2019**, *31*, 1802120.
(63) Kaneko, T.; Tanaka, S.; Asao, N.; Yamamoto, Y.; Chen, M.; Zhang, W.; Inoue, A. Reusable and Sustainable Nanostructured Skeleton Catalyst: Heck Reaction with Nanoporous Metallic Glass Pd (PdNPore) as a Support, Stabilizer and Ligand-Free Catalyst. *Adv. Synth. Catal.* **2011**, *353*, 2927−2932.
(64) Doubek, G.; Sekol, R. C.; Li, J.; Ryu, W.-H.; Gittleson, F. S.; Nejati, S.; Moy, E.; Reid, C.; Carmo, M.; Linardi, M.; Bordeenithikasem, P.; Kinser, E.; Liu, Y.; Tong, X.; Osuji, C. O.; Schroers, J.; Mukherjee, S.; Taylor, A. D. Guided Evolution of Bulk Metallic Glass Nanostructures: A Platform for Designing 3D Electrocatalytic Surfaces. *Adv. Mater.* **2016**, *28*, 1940−1949.
(65) Kinser, E. R.; Padmanabhan, J.; Yu, R.; Corona, S. L.; Li, J.; Vaddiraju, S.; Legassey, A.; Loye, A.; Balestrini, J.; Solly, D. A.; Schroers, J.; Taylor, A. D.; Papadimitrakopoulos, F.; Herzog, R. I.; Kyriakides, T. R. Nanopatterned Bulk Metallic Glass Biosensors. *ACS Sens* **2017**, *2*, 1779−1787.
(66) Zhang, P.; Wang, Z.; Perepezko, J. H.; Voyles, P. M. Vitrification, Crystallization, and Atomic Structure of Deformed and Quenched $Ni_{60}Nb_{40}$ Metallic Glass. *J. Non-Cryst. Solids* **2018**, *491*, 133−140.
(67) Yang, L.; Meng, X.-f.; Guo, G.-q. Structural Origin of the Pinpoint-Composition Effect on the Glass-Forming Ability in the NiNb Alloy System. *J. Mater. Res.* **2013**, *28*, 3170−3176.
(68) Enayati, M. H.; Dastanpoor, E. Comparative Study of Mechanical Alloying Induced Nanocrystallization and Amorphization in Ni-Nb and Ni-Zr Systems. *Metall. Mater. Trans. A* **2013**, *44*, 3984−3998.
(69) Enayati, M. H.; Schumacher, P.; Cantor, B. The Structure and Thermal Stability of Mechanically Alloyed Ni-Nb-Zr Amorphous Alloys. *J. Mater. Sci.* **2002**, *37*, 5255−5259.
(70) Luo, W. K.; Sheng, H. W.; Alamgir, F. M.; Bai, J. M.; He, J. H.; Ma, E. Icosahedral Short-Range Order in Amorphous Alloys. *Phys. Rev. Lett.* **2004**, *92*, 145502/1−145502/4.
(71) Sun, L.; He, J. H.; Sheng, H. W.; Searson, P. C.; Chien, C. L.; Ma, E. Magnetic Properties of Amorphous $Ni_{60}Ag_{40}$ Films. *J. Non-Cryst. Solids* **2003**, *317*, 164−168.
(72) Lee, W. S.; Kim, S. C.; Yoon, W. Y.; Kwun, S. I. Mechanical Alloying Behaviors of the $Ni_{50}Ti_{50}$ System by Pulverization. *Taehan Kumsok Hakhoechi* **1996**, *34*, 886−896.
(73) Twohig, E.; Tiernan, P.; Butler, J.; Dickinson, C.; Tofail, S. A. M. Mechanical, microstructural and thermal properties of a 50:50 at.% nickel-titanium alloy subjected to a dieless drawing process. *Acta Mater.* **2014**, *68*, 140−149.
(74) Plummer, J. Is Metallic Glass Poised to Come of Age? *Nat. Mater.* **2015**, *14*, 553−555.
(75) Collins, L. E.; Grant, N. J.; Vander Sande, J. B. Crystallization of Amorphous Nickel-Niobium ($Ni_{60}Nb_{40}$). *J. Mater. Sci.* **1983**, *18*, 804−814.
(76) Trifonov, A. S.; Lubenchenko, A. V.; Polkin, V. I.; Pavolotsky, A. B.; Ketov, S. V.; Louzguine-Luzgin, D. V. Difference in Charge Transport Properties of Ni-Nb Thin Films with Native and Artificial Oxide. *J. Appl. Phys.* **2015**, *117*, 125704/1−125704/5.
(77) Chellali, M. R.; Nandam, S. H.; Li, S.; Fawey, M. H.; Moreno-Pineda, E.; Velasco, L.; Boll, T.; Pastewka, L.; Kruk, R.; Gumbsch, P.; Hahn, H. Amorphous Nickel Nanophases Inducing Ferromagnetism in Equiatomic Ni-Ti Alloy. *Acta Mater.* **2018**, *161*, 47−53.
(78) Chen, N.; Shi, X.; Witte, R.; Nakayama, K. S.; Ohmura, K.; Wu, H.; Takeuchi, A.; Hahn, H.; Esashi, M.; Gleiter, H.; Inoue, A.; Louzguine, D. V. A Novel Ti-Based Nanoglass Composite with Submicron-Nanometer-Sized Hierarchical Structures to Modulate Osteoblast Behaviors. *J. Mater. Chem. B* **2013**, *1*, 2568−2574.
(79) Bag, S.; Baksi, A.; Wang, D.; Kruk, R.; Benel, C.; Chellali, M. R.; Hahn, H. Combination of Pulsed Laser Ablation and Inert Gas

https://dx.doi.org/10.1021/acsnano.9b09778
ACS Nano 2020, 14, 5543−5552

Condensation for the Synthesis of Nanostructured Nanocrystalline, Amorphous and Composite Materials. *Nanoscale Adv.* **2019**, *1*, 4513–4521.

https://dx.doi.org/10.1021/acsnano.9b09778
ACS Nano 2020, 14, 5543–5552